Azimuthal Uniformity of Cylindrical Implosions on OMEGA

D. H. Barnak,[1] M. J. Bonino,[1] P.-Y. Chang,[2] J. R. Davies,[1] E. C. Hansen,[3] D. R. Harding,[1] J. D. Moody,[4] J. L. Peebles,[1] B. B. Pollock,[4] and R. Betti[1]

[1]Laboratory for Laser Energetics, University of Rochester
[2]Institute of Space and Plasma Sciences, National Cheng Kung University, Taiwan
[3]Department of Physics and Astronomy, University of Rochester
[4]Lawrence Livermore National Laboratory

Introduction

Magnetized liner inertial fusion (MagLIF) employs a cylindrical implosion to compress magnetized preheated fuel to fusion-relevant conditions. The MagLIF concept was originally designed around a Z-pinch compression,[1,2] which is naturally uniform barring instabilities that form at the inner and outer surfaces.[3–5] To adapt the MagLIF concept to a laser-driven platform, a beam-pointing scheme that achieves a uniform cylindrical implosion must be established. Direct-drive cylindrical implosion platforms have been developed using the OMEGA laser[6] with the interest of studying Rayleigh–Taylor instability growth[7,8] and magnetic-flux compression[9] in cylindrical geometry. Such designs employed in the past have demonstrated axial and azimuthal uniformity with measurements and simulations.[10] Unfortunately, the aspect ratio of the laser-driven MagLIF targets and available distributed phase plates prohibit using these experimental designs.

The axial pointing is empirically derived[11,12] since many effects, such as cross-beam energy transfer[13,14] and angle of incidence dependence on laser absorption, complicate finding an analytic solution; an axially uniform illumination does not result in an axially uniform implosion. Calculating azimuthal uniformity has no such complications; an azimuthally uniform illumination gives an azimuthally uniform implosion. Using a finite number of beams will always have some nonuniformity in the illumination of a cylinder, so it is important to quantify how these perturbations affect the drive symmetry. The geometry of the OMEGA laser[15] has four rings of ten beams available to use for a cylindrical implosion, which means at the very least there will be some mode-10 perturbation imposed by the illumination pattern.

Experimental Setup

The standard pointing experiments used parylene-N plastic cylinders that were coated on machined and polished stainless-steel mandrels to 20-, 24-, and 30-μm thicknesses and an 11- to 14-atm fill of D_2 gas. Outer diameters ranged from as low as 550 μm to as high as 610 μm. The shell shape was determined from end-on self-emission x-ray images of the shell in flight. Given the view of the camera and opacity effects from the target, the self-emission images represent the drive uniformity from the ten beams closest to the camera. The laser energy in that group of beams was raised and lowered accordingly to achieve axial uniformity on the cylinder, but the azimuthal uniformity measured by the x-ray images depends only on the distribution and relative intensities of individual beams. The relative imbalance between adjacent beams in the group is no more than 5% rms and does not affect the azimuthal illumination pattern on the cylinder.

The uniform pointing experiments utilized Rexolite tubes with no gas fill, an outer diameter of 640 μm, and 30-μm thickness. Shell shape was determined by x-ray self-emission as before, but in these recent experiments, used the uniform pointing calculated from illuminating the 600-μm-diam hard cylinder. The energy in all of the beams was fixed to ensure axial uniformity, and the imbalance between subsequent beams was, at most, 2% rms. The difference in the imposed perturbation between the 600-μm

and 640-μm cylinders is small enough to be insignificant, but since it is larger, it can infer that smaller-diameter targets will have the same degree of uniformity or better.

The differences between the standard and uniform pointing used and the outer diameters of the target are highlighted by calculating the hard cylinder illumination profile, as shown in Fig. 1. A lineout of each illumination pattern is taken through the beam centers from the ring of beams that drives the end of the cylinder imaged in the radiographs. The lineout is then decomposed into cylindrical modes using Fourier's trick. The amplitude of the nth mode, A_n, is

$$A_n = \frac{1}{\pi}\int_0^{2\pi} F(\theta)e^{-\mathrm{in}\theta}\,\mathrm{d}\theta, \tag{1}$$

where $F(\theta)$ is the lineout in angular space. Note that to have only positive modes, the mode amplitudes must be normalized to $1/\pi$. From this analysis we can compare the mode-5 and mode-10 amplitudes for the standard beam pointing on the nominal 600-μm cylinder, the uniform pointing on the same outer diameter, and the adjusted pointing on the 640-μm cylinder in Fig. 2. All other cylinder mode amplitudes are a fraction of a percent comparatively in these cases.

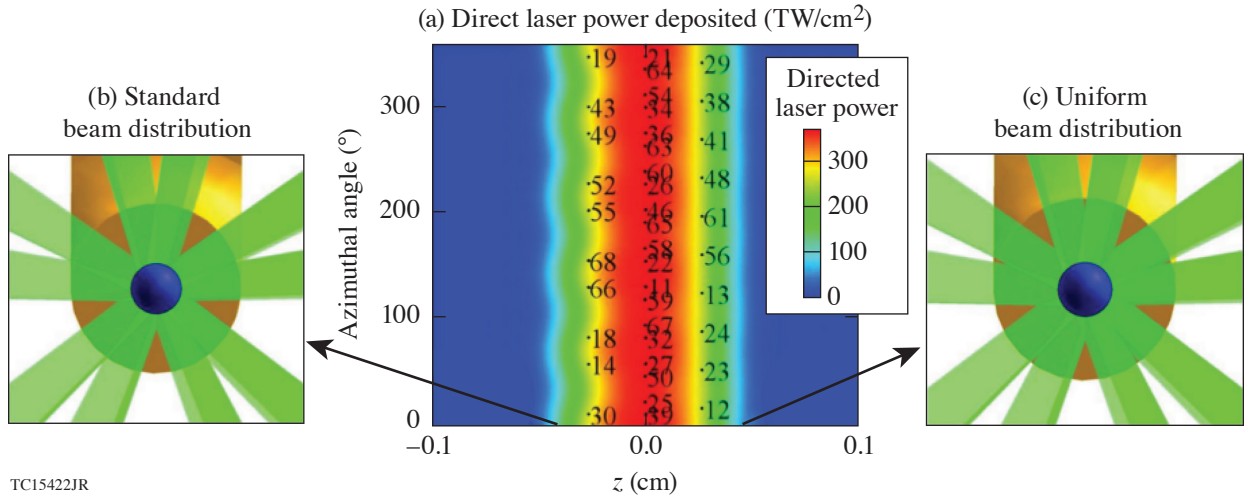

Figure 1
Pointing configuration of the standard and adjusted uniform pointing. (a) The total laser power deposited on the surface of a 600-μm-outer-diam hard cylinder. [(b),(c)] The beams that drive the end of the cylinder closest to the observer, with the cylinder axis coming out of the page. This view of the cylinder is congruent with the view of the framing camera that captured the images of the cylindrical shell in flight. The difference between the two pointings is visually imperceptible; however, this small shift reduces the overall mode-5 perturbation.

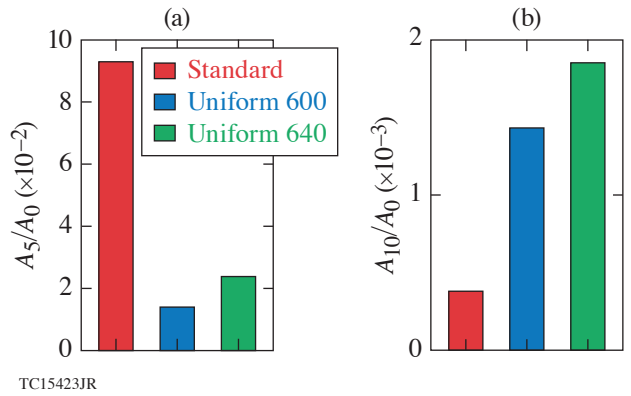

Figure 2
Initial cylindrical mode amplitudes for (a) mode 5 and (b) mode 10 for the standard pointing and the uniform pointing for a 600-μm-outer-diam cylinder and a 640-μm-outer-diam cylinder. The total sum difference between the uniform and standard pointing is a decrease in the mode-5 amplitude by a factor of 6 and an increase in the mode-10 amplitude by a factor of 4. Mode 5 still remains the dominant perturbation.

Standard Pointing Results

Measurements taken with the x-ray framing camera provide time-resolved measurements of the cylindrical mode amplitude growth. Representative images for the three different shell thicknesses used in the standard pointing experiment are shown in Fig. 3. The mode amplitudes are then calculated from the average azimuthal lineout using Fourier's trick, as seen for the irradiation profile in Eq. (1). The modes calculated from the integral are normalized by the mode-0 amplitude, which is

$$A_0 = \int_0^{2\pi} \frac{1}{2\pi} F(\theta)\,\mathrm{d}\theta \tag{2}$$

and is dependent on the camera settings and other hard-to-quantify values such as charge-coupled-device response and gain droop across the strip. Mode 5 is the dominant mode seen growing over time for almost all cases, except for a few cases where there instead appears to be a mode 6. It is difficult to reason why a mode-6 growth would be preferred, given the shape of the initial nonuniformity imposed by the laser, but it is not unreasonable to assume that a target defect or some other feature in the target is responsible.

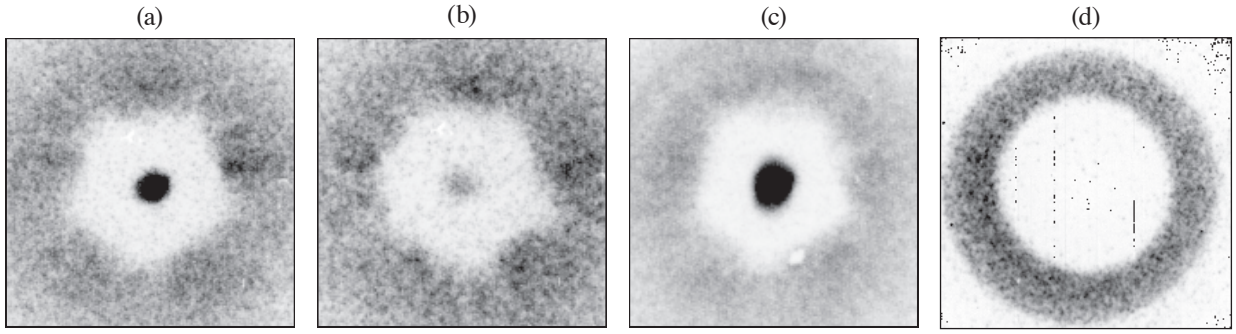

Figure 3
Representative sample images of the cylindrical shell in flight for the standard pointing for (a) 30 μm, (b) 24 μm, and (c) 20 μm. A pentagon structure is visible an all three images. The image sizes are twice the size of the centering circle's diameter, so the image is averaged radially over 70% of the image presented. The 24-μm shell in (b) shows a slight deformation on the left side of the pentagon, which is reflected in the analysis as a growing mode-6 amplitude. (d) A sample x-ray radiograph of a 30-μm-thick, 635-μm-OD cylinder driven by the uniform pointing shows the shell shape staying round to within ±10 μm.

The briefest and most-complete summary of the results from the standard pointing is that regardless of cylinder diameter and shell thickness, if a mode-5 perturbation of sufficient amplitude is imposed by the laser drive, a mode-5 perturbation will grow. The question of what constitutes a sufficient amplitude will be covered in **Uniform Pointing Results** (p. 127). The amplitude of the perturbation is 6.7% for the smallest outer diameters and 9.3% for the largest outer diameters. The modes grow linearly in time since the acceleration of the ablation surface against the denser shell is stable. The shape of the implosion imposed by the laser likely seeds deceleration-phase Rayleigh–Taylor perturbations after the drive has been turned off. The reduction in mode amplitude from smaller-OD targets does not affect the amplitude growth rate of mode 5 to within the error bars as shown in Fig. 4. Mode-5 growth is also uncorrelated with shell thickness and initial gas pressure.

Three-Dimensional *HYDRA* Simulations

Simulations using the radiation-hydrodynamic code *HYDRA* were used to produce synthetic radiographs of four configurations: (1) a 30-μm-thick, 600-μm-OD shell driven with a 2.0-ns-long pulse using the standard beam pointing; (2) a 20-μm-thick, 580-μm-OD shell with the same laser drive as case 1; (3) a 30-μm-thick, 640-μm-OD shell driven by a 1.5-ns-long pulse using the uniform pointing; and (4) a 20-μm-thick, 580-μm-OD shell with the same laser drive as case 3.

Self-emission x-ray images from the end of the cylinder are generated in a post-processing routine using the Yorick interpreted language.[16] The simulated radiographs for both pointing cases for 30-μm and 20-μm shells are shown in Fig. 5. Each image is calculated from opacity and emissivity tables along the cylindrical axis line of sight using 0.01- to 10-keV x rays and including the transmission of a 25.4-μm-thick Be filter to match the filters used in the experiment. The image has a field of view of 600 ×

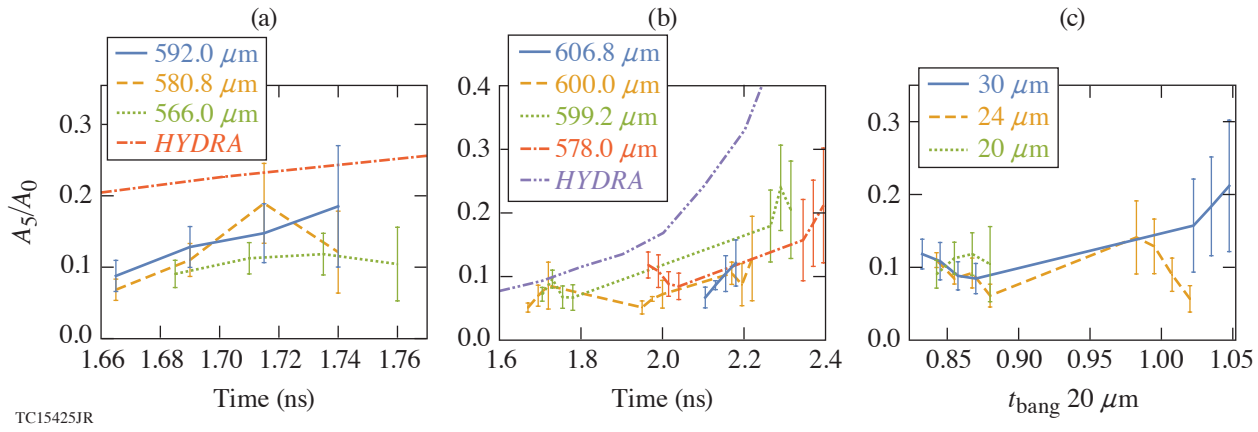

Figure 4
Plots of mode-5 growth for (a) 20-μm and (b) 30-μm-thick cylinders. Between the two thicknesses, different outer diameters do not have a statistically relevant trend of having higher or lower mode-5 perturbation growth over time. *HYDRA* simulations predict a faster mode growth and larger mode amplitude close to the peak x-ray emission of the core. (c) Plots for mode-5 amplitude plotted as a function of time normalized to the x-ray bang time of the 20-μm-thick shells demonstrate that the mode-5 amplitude does not depend on shell thickness.

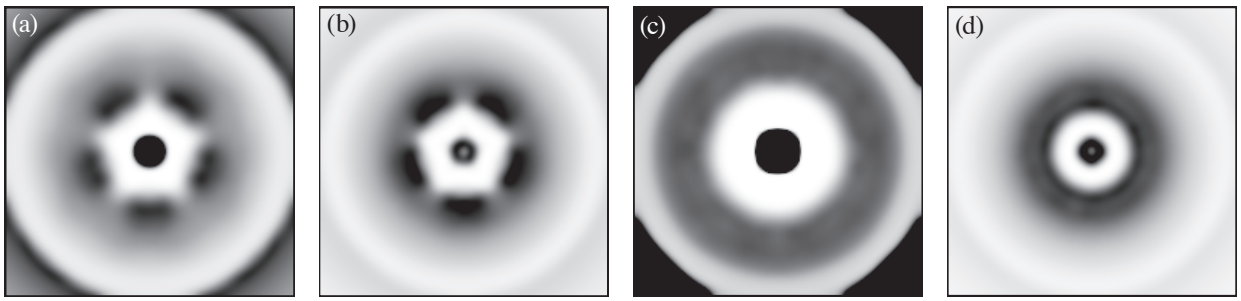

Figure 5
Images of *HYDRA* simulated x-ray radiographs of the standard pointing for (a) a 30-μm and (b) a 20-μm shell and the uniform pointing for (c) a 30-μm and (d) a 20-μm shell. The radiographs for the standard pointing exhibit the same pentagonal structure as the experimental radiographs. The uniform pointing radiographs are round to ±1 pixel, which is the same as the experiment.

600 μm resolved by 200 × 200 pixels. Each image is convolved with the same point-spread function associated with the framing cameras and is processed identically to the experimental images, which is described in the previous sections. Since the images are free of noise, no error bars are reported for the mode amplitudes recovered from simulations. Residuals from the fit of Fourier decomposition to the simulated azimuthal profile are too small to represent graphically.

Uniform Pointing Results

The simulations are plotted with the experimental results for the uniform pointing in Fig. 6. Unfortunately, there are no experimental data for the 20-μm shells in this case. The briefest and most-complete summary of the uniform pointing shots is that there is no longer a mode-5 growth shown in Fig. 6 or a mode 10 imposed from the adjustments as shown in Fig. 6. The degree of uniformity of the implosion is best shown by the radiograph in Fig. 3(d).

Conclusions

Azimuthal uniformity was calculated analytically by shifting the beams to minimize the mode-5 perturbation from the standard pointing of the OMEGA laser. Data taken using the standard pointing show that, independent of cylinder outer diameter and shell thickness, a mode-5 perturbation grows as a result of the mode-5 asymmetry from the drive. The lowest-possible amplitude that gives a pentagonal-shaped shell is 6.7%, which is inferred from the different cylinder outer diameters used in the experiment.

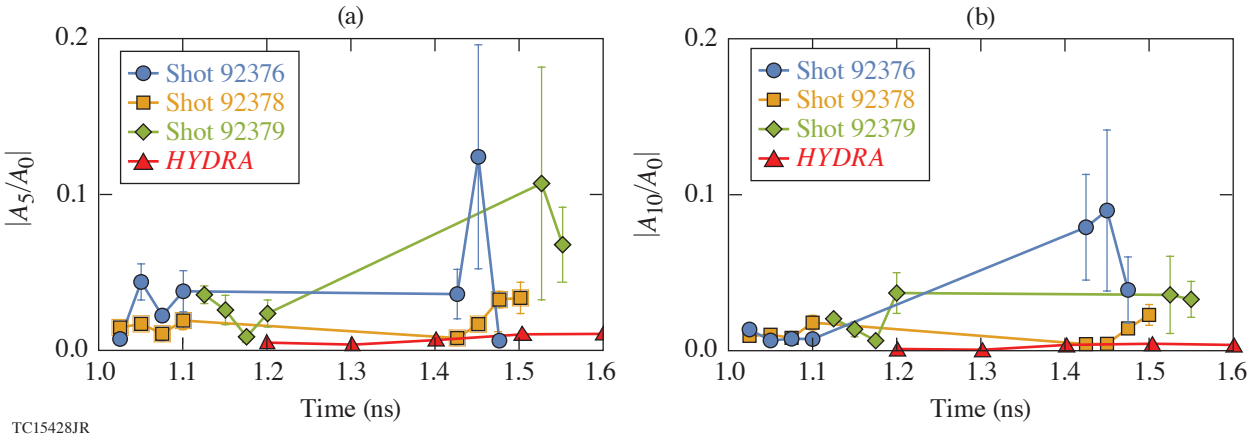

Figure 6
(a) Mode-5 and (b) mode-10 amplitudes for 30-μm-thick shells for the uniform laser drive. The *HYDRA* predictions of the mode-5 and mode-10 amplitudes for the 30-μm shells are well below the measurements later in time. The 20-μm-thick shells (not shown) have similar results from *HYDRA*.

The adjustment made to the standard pointing reduces this initial perturbation to 2.2%, which completely eliminates the observed mode 5. The increase of mode 10 as a result of this adjustment is less than the mode-5 amplitude at 2%, and no mode-10 growth on the shell is observed. The experiments are reproduced using 3-D *HYDRA* simulations, although the perturbation amplitude is overestimated for the standard pointing case. Both simulations and experiments show that the uniform pointing gives a circular implosion to within a 10-μm resolution.

The information, data, or work presented herein was funded in part by the Advanced Research Projects Agency-Energy (ARPA-E), U.S. Department of Energy, under Award No. DE-AR0000568, the Department of Energy National Nuclear Security Administration under Award No. DE-NA0001944, DE-NA0003856, and in part under contract 89233218CNA000001, the U.S. Department of Energy Office of Inertial Confinement Fusion under Cooperative Agreement No. DE-FC52-08NA28302, the University of Rochester, and the New York State Research and Development Authority. Los Alamos National Laboratory, an affirmative action/equal opportunity employer, is operated by Triad National Security, LLC for the National Nuclear Security Administration of U.S. Department of Energy under contract 89233218CNA000001.

1. S. A. Slutz *et al.*, Phys. Plasmas **17**, 056303 (2010).
2. S. A. Slutz and R. A. Vesey, Phys. Rev. Lett. **108**, 025003 (2012).
3. K. J. Peterson *et al.*, Phys. Plasmas **20**, 056305 (2013).
4. K. J. Peterson *et al.*, Phys. Rev. Lett. **112**, 135002 (2014).
5. K. J. Peterson *et al.*, Phys. Plasmas **19**, 092701 (2012).
6. C. W. Barnes *et al.*, Rev. Sci. Instrum. **70**, 471 (1999).
7. D. Tubbs *et al.*, Laser Part. Beams **17**, 437 (1999).
8. J. P. Sauppe *et al.*, Matter Radiat. Extremes **4**, 065403 (2019).
9. O. V. Gotchev *et al.*, Phys.Rev. Lett. **103**, 215004 (2009).
10. J. P. Sauppe *et al.*, Phys. Plasmas **26**, 042701 (2019).
11. E. C. Hansen *et al.*, Plasma Phys. Control. Fusion 60, 054014 (2018).

12. E. C. Hansen *et al*., Phys. Plasmas **25**, 122701 (2018).

13. A. K. Davis *et al*., Phys. Plasmas **23**, 056306 (2016).

14. V. N. Goncharov *et al*., Plasma Phys. Control. Fusion **59**, 014008 (2016).

15. R. S. Craxton, Laboratory for Laser Energetics Report No. DOE/DP 40200-101, University of Rochester (1989).

16. D. H. Munro and P. F. Dubois, Comp. Phys. **9**, 609 (1995).